

RESEARCH ARTICLE

Separations: Materials, Devices and Processes

Molecule transfer mechanism in two-dimensional heterostructured lamellar membranes: The effects of dissolution and diffusion

Chongchong Chen¹ | Xiaoli Wu^{1,2} | Jie Zhang¹ | Jingjing Chen¹ | Xulin Cui¹ |
Wenpeng Li¹ | Wenjia Wu¹ | Jingtao Wang^{1,2} 

¹School of Chemical Engineering, Zhengzhou University, Zhengzhou, People's Republic of China

²Henan Institute of Advanced Technology, Zhengzhou University, Zhengzhou, People's Republic of China

Correspondence

Jingtao Wang, School of Chemical Engineering, Zhengzhou University, Zhengzhou 450001, People's Republic of China.
Email: jingtaowang@zzu.edu.cn

Funding information

Henan Natural Science Funds for Excellent Young Scholar, Grant/Award Number: 202300410373; National Natural Science Foundation of China, Grant/Award Number: U2004199; Natural Science Foundation of Henan Province, Grant/Award Number: 212300410285

Abstract

Two-dimensional lamellar membranes are promising for efficient molecule transfer, while the underlying transfer mechanism is rarely elucidated. Herein, heterostructured nanosheets are prepared by self-assembling small-sized hydrophilic cyanuric acid melamine and hydrophobic *g*-C₃N₄ nanosheets. Resultant lamellar membranes show comparable affinity to polar and nonpolar solvents, allowing them to dissolve on membrane surface and diffuse through membrane channels. Results demonstrate that for lamellar membranes with distinct wettability, the permeance difference for polar solvents is originated from dissolution and diffusion processes, while that for nonpolar solvents is stemmed from dissolution process. Accordingly, corresponding equations which are suitable for heterostructured lamellar membranes are established. Importantly, polar solvents are induced to form ordered arrangement in hydrophilic nanodomains and then maintain the ordered state in hydrophobic nanodomains, affording a low-resistance transfer and high acetonitrile permeance of 1025 L m⁻² h⁻¹ bar⁻¹. In contrast, nonpolar solvents with disordered arrangement exhibit lower permeance than that of polar ones.

KEYWORDS

dissolution and diffusion, hydrophilic/hydrophobic heterostructured nanosheet, lamellar membrane, transfer mechanism, transfer rate equation

1 | INTRODUCTION

The newly developed two-dimensional (2D) lamellar membranes with well-defined nanostructures display fast molecule transfer and precise sieving, attracting ever-increasing attention in a wide range of applications including gas capture, water purification and organics recovery, and so on.^{1–4} For instance, MXene lamellar membrane with regular channels exhibits low-resistance molecule transport and high water permeance over 1000 L m⁻² h⁻¹ bar⁻¹, which is more than 2 orders

of magnitude higher than that of state-of-the-art polymer membranes.^{5–7} The current studies of lamellar membrane are mainly focused on manipulating the nanostructures of membrane surface and interlayer channels to enhance molecule permeation.^{8–11} While the underlying molecule transfer mechanism remains to be fully elucidated. Traditional viewpoint deems that molecule transfer is governed by viscosity that obeys Poiseuille's law, when molecules display classical continuum flow for membrane channels with the size of a few nanometers.^{12–14} Recently, it has been demonstrated that the transfer is also affected by molecule kinetic diameter and solubility parameter, based on which the transfer equations can be established.¹⁵

Chongchong Chen and Xiaoli Wu contributed equally to this work.

Nevertheless, the dissolution-diffusion mechanism, which is a typical theory to describe molecule transfer in polymer membranes, has yet been utilized in the investigation for lamellar membranes.

Previous studies have demonstrated that, by regulating the microstructure of membrane surface and channels, molecule dissolution and diffusion ability can be altered. And then the molecule transfer rate in lamellar membrane can be adjusted.^{16–20} For example, Jiang and co-workers found that the permeance of polar and nonpolar solvents can be significantly elevated when spraying hydrophilic and hydrophobic polymer clusters on membrane surface, respectively, which led to enhanced molecule dissolution ability. As a result, the permeance of water and n-hexane was improved from 15.0 and 19.0 L m⁻² h⁻¹ bar⁻¹ to 98.1 and 143.6 L m⁻² h⁻¹ bar⁻¹, respectively.¹⁶ In addition, Thebo et al. achieved two orders of magnitude higher water permeance in comparison with primary GO membrane by intercalating theanine amino acid in the channels to manipulate molecule diffusion ability.¹⁸ Differently, Wang and co-workers elevated toluene permeance by less than 1.5 times from 38.5 to 53.3 L m⁻² h⁻¹ bar⁻¹ by inserting sodium chloride into GO membrane channels.²⁰ Analogously, it has been demonstrated that polar solvents in hydrophilic channels form orderly aligned aggregates along channel walls. In contrast, nonpolar solvents are disorderly distributed in hydrophilic channels and diffuse slowly.²¹ This indicates that molecule diffusion in channels exerts distinct effects on transport behavior of polar and nonpolar solvents. Despite these breakthroughs, there is no explicit cognition about the main factor that induces the transfer discrepancy in lamellar membranes with distinct wettability, and the transfer mechanism is still controversial. One basic reason is that the conventional lamellar membranes, which are often assembled by hydrophilic or hydrophobic nanosheets, exhibit distinct affinity to polar and nonpolar solvents.^{22,23} Especially, the low affinity would repel the dissolution of molecules on membrane surface, thus confounding the effect of diffusion on transfer efficiency. Thus, a platform with comparable affinity is highly desirable for exploring the underlying molecule transfer mechanism.

Hydrophilic/hydrophobic heterostructured nanomaterials, which subtly synergize two materials with reversed hydrophilicity/hydrophobicity, have attracted wide research interest.^{24–27} Heterostructured lamellar membrane with tunable chemical components holds potential for comparable affinity toward both polar and nonpolar solvents, affording equivalent opportunity for them to dissolve on membrane surface and to diffuse in channels. Therefore, heterostructured lamellar membrane is a desirable platform for exploring molecule transfer mechanism. One recent work designed heterostructured lamellar membrane by adding hydrophobic *g*-C₃N₄ nanosheets into hydrophilic GO interlamination, resulting in 10-time boosted water permeance.²⁸ However, the interlayer channels are often disordered and difficult to be modulated precisely. In contrast, heterostructured lamellar membrane assembled by hydrophilic/hydrophobic heterostructured nanosheets provides promising platform yet remains rarely adopted for studying molecule transfer mechanism.

Herein, heterostructured nanosheets containing small-sized hydrophilic cyanuric acid melamine (CMN) nanodomains and

hydrophobic *g*-C₃N₄ nanodomains were designed as building blocks to assemble heterostructured lamellar membranes. The microstructures and physicochemical properties of membranes were investigated in detail. Based on this novel platform, molecule transfer mechanism was systematically investigated based on water and organic permeation. We demonstrate that for lamellar membranes with distinct wettability, the transfer discrepancy of polar solvents is originated from both dissolution and diffusion processes, while that of nonpolar solvents is mainly stemmed from dissolution process. The corresponding equations are established. In addition, heterostructured lamellar membrane achieves significantly enhanced permeance for polar solvents, originating from the excellent dissolution on membrane surface and ultrafast diffusion in channels. The permeance for acetonitrile reaches 1025 L m⁻² h⁻¹ bar⁻¹. In contrast, nonpolar solvents acquire relatively lower permeance in comparison with that of polar ones. Furthermore, the well-designed interlayer channels ensure accurate sieving and excellent structural stability of lamellar membranes. The effects of dissolution and diffusion processes on molecule transfer behavior are elucidated, which is instructive for the development of advanced lamellar membranes.

2 | MATERIALS AND METHODS

2.1 | Materials

Nylon microfiltration substrate with 0.2 μm pore size and 50 mm diameter was purchased from Tianjin Jinteng Experimental Equipment Co., Ltd. Melamine and cyanuric acid were supplied from Shanghai Macklin Biochemical Co., Ltd. Concentrated HCl (35%–37% wt% in water) was obtained by Sinopharm Chemical Reagent Co. Ltd., China. Polydimethylsiloxane (PDMS) was purchased from 3A Chemicals Co., Ltd. Dopamine and *Tris* were supplied by Beijing HWRK Chem Co., Ltd. Organic solvents (acetonitrile, acetone, methanol, isopropanol [IPA], ethyl acetate, ethanol, n-octane, n-heptane, n-pentane, n-hexane, and toluene) were obtained from Tianjin Kemiou Chemistry Reagent Co., Ltd. Acid yellow 14 (AY14), brilliant blue (BB), reactive red (RR), crystal violet (CV), methylene blue (MB), methyl orange (MO), and rose bengal (RosB) were supplied from Aladdin Chemical Co., Ltd. These were used as received without further treatment, and deionized water was used throughout the experiment.

2.2 | Preparation of heterostructured nanosheets

The small-sized hydrophobic *g*-C₃N₄ nanosheets were obtained by liquid exfoliating of as-prepared *g*-C₃N₄ powder in IPA.^{29,30} In detail, 50 mg of *g*-C₃N₄ powder was uniformly dispersed in 100 ml of IPA. Then, the solution was sonicated for about 16 h and subsequently centrifuged at 6000 rpm to remove residual unexfoliated *g*-C₃N₄ nanoparticles and large-size nanosheets. The lateral size of nanosheets was accurately controlled by tuning the ultrasonic time and centrifugal speed. The small-sized hydrophilic nanosheets were

fabricated by classic cyanuric acid and melamine self-assembly.³¹ In detail, 2.0 g of mixture of cyanuric acid and melamine with a molar ratio of 1:1 was dissolved in 100 ml of ethanol to ensure horizontal growth. Then, they were mixed for 1 h using automatic shaker at 30°C. The mixture was washed several times with ethanol to remove unpolymerized cyanuric acid and melamine. The resultant powder was vacuum dried at 60°C. Then, 50 mg of powder was uniformly dispersed in 100 ml of IPA and sonicated for 10 min, and then the dispersion was centrifuged at 6000 rpm to remove large-area nanosheets. Meanwhile, the heterostructured nanosheets were fabricated by a self-assembled strategy. In detail, 50 ml of $g\text{-C}_3\text{N}_4$ nanosheets supernatant solution was uniformly mixed with 50 ml of hydrophilic CMN supernatant liquid and stirred for 1 h at 40°C. Importantly, the pH of the mixed dispersion was adjusted to 5.0 by HCl solution to improve the accepting ability of carbonyl groups for nucleophile reagent. Then, the reaction mixture was centrifuged at 5000 rpm and then washed with IPA to pH = 7.0, obtaining the light-yellow powder. Ten milligrams of nanosheet powder were uniformly dispersed in 100 ml of IPA and then sonicated for 5 min to obtain uniform solution with a concentration of 0.1 mg ml⁻¹.

2.3 | Preparation of lamellar membranes

The lamellar membranes with well-defined channels were prepared via variable speed vacuum filtration (pressure, 0.2–1.0 bar) of nanosheets dispersion on the top of Nylon microfiltration support. To improve the affinity between the Nylon support and nanosheets, the support was pre-treated with dopamine aqueous solution (2 mg ml⁻¹) with 10 mM of *Tris*-HCl for 4 h to deposit polydopamine (PDA) layer.^{32,33} Moreover, to prepare high-quality lamellar membranes, 7 ml of initial nanosheet solution was diluted to 200 ml by IPA for a low concentration of 0.0035 mg ml⁻¹. And this diluted solution was filtrated on Nylon support to prepare heterostructured lamellar membranes. At the end of filtration, the obtained membrane was immediately immersed in organic solvent to maintain a solvated state.^{4,13} The PDMS/ $g\text{-C}_3\text{N}_4$ and PDMS/CMN membranes were fabricated by a similar method. First, PDMS solution (0.1 wt%) was obtained by dissolving in the mixture of ethanol and n-hexane (4:3, w/w). Afterward, the PDMS solution (10 ml) was sprayed, respectively, on CMN and $g\text{-C}_3\text{N}_4$ membrane surfaces.

2.4 | Evaluation of nanofiltration performance

Nanofiltration performance was evaluated on a home-made device by measuring the permeance of various solvents and rejection of dyes respectively. The physical properties of used solvents are shown in Table S2, and the dyes were dissolved in methanol solvent for rejection test. To ensure the comparability of nanofiltration performance, membranes with the same thickness were selected to conduct the testing. Prior to the testing, the membrane was immersed in the experiment solvents for 24 h to achieve an equilibrium state. And the

related experiments were carried out under N₂ pressure of 1–7 bar with the effective membrane area of 7.0 cm². Note that dye molecules with distinct sizes were dissolved in methanol to obtain the desired concentration (10 mg L⁻¹) for rejection measurement, and the concentration was analyzed by NanoDrop UV-vis spectrophotometer. The solvent permeance (P , L m⁻² h⁻¹ bar⁻¹) was calculated as the following equation:

$$P = \frac{V_p}{(A \cdot t \cdot \Delta P)}, \quad (1)$$

where V_p , A , t , and ΔP represent the permeate volume (L), effective membrane area (m²), testing time (h), and operating pressure (bar), respectively. The rejection (R , %) was obtained by using the following equation:

$$R = \left(1 - \frac{C_p}{C_f}\right) \times 100, \quad (2)$$

where C_p and C_f denote the concentration of permeate side solution and feed solution, respectively. All tests were performed at room temperature through three parallel membranes and the obtained data were averages of three tests.

2.5 | Characterization

The morphology and thickness of nanosheets and membranes were characterized by scanning electron microscopy (SEM, Auriga FIB SEM, Zeiss, Germany) and atomic force microscopy (AFM, Bruker Dimension Fast Scan). The lattice of nanosheet was further observed by high-resolution transmission electron microscopy (HRTEM, Tecnai G2 F20, FEI, USA). In addition, chemical compositions of nanosheets and membranes were detected by energy-dispersive spectroscopy (EDS) on Auriga FIB SEM, X-ray photoelectron spectroscopy (XPS, AXIS Supra, Kratos, UK) and Fourier transform infrared (FTIR) with the wavelength from 400 to 4000 cm⁻¹ (Nicolet MAGNA-IR560 instrument). X-ray diffraction (XRD) was measured on Bruker D8 Advance ECO with the solvated state of membrane samples. N₂ adsorption isotherms were tested for the membranes on automated gas sorption analyzer (Quantachrome Ltd., America). Moreover, the contact angle was tested with FACE (model OCA 25, Germany) at room temperature.

3 | RESULTS AND DISCUSSION

3.1 | Characterization of heterostructured nanosheet

The heterostructured CM/ C_3N_4 nanosheets were prepared by self-assembling small-sized hydrophilic CMN and hydrophobic $g\text{-C}_3\text{N}_4$ nanosheets in weakly acidic IPA solution (Figure 1A; Figure S2).

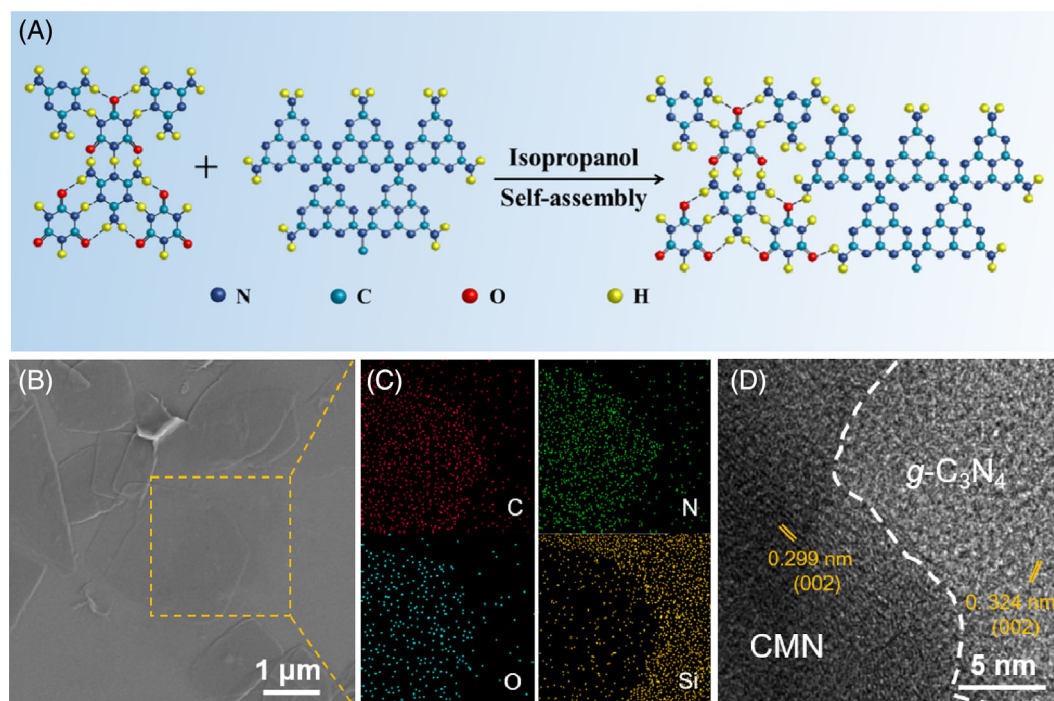


FIGURE 1 Proofs for the synthesis of heterostructured CM/C₃N₄ nanosheet. (A) Schematic illustration of the assemble process for CM/C₃N₄ nanosheet. (B) Scanning electron microscopy image, (C) corresponding elemental mappings of C, N, O, and Si, and (D) high-resolution transmission electron microscopy image of CM/C₃N₄ nanosheet

During the preparation process, amino groups on the edges of *g*-C₃N₄ nanosheets bonded with hydroxyl/carbonyl groups on the edges of CMN nanosheets through Schiff base reaction and hydrogen-bonding interactions, as proved by FTIR and XPS. Figure S3 shows that compared with primary CMN, the enhanced intensity of C=N peak on CM/C₃N₄ suggests the Schiff base reaction between amino and carbonyl groups. Besides, this peak exhibits a red shift from 1670 to 1630 cm⁻¹, verifying the formation of hydrogen bonds between nanosheets.^{34,35} This is further confirmed by the increment of sp²-bonded N in triazine rings (C=N=C) at 398.7 eV and the decrement of terminal amino groups (—NH₂/—NH—) at 401.3 eV in XPS spectra (Figure S4). This mild reaction allows well-maintaining sheet structure of CM/C₃N₄ without visible holes and bulges, as confirmed by SEM and AFM images (Figure 1B; Figure S5). CM/C₃N₄ nanosheets possess typical 2D structure with lateral size of ~2 μm and height of ~1.1 nm. Considering that the lateral sizes of CMN and *g*-C₃N₄ nanosheets are ~92 and 87 nm, respectively, CM/C₃N₄ nanosheet is probably bonded by ~10 pieces of CMN and *g*-C₃N₄ nanosheets alternately with edge-to-edge structure (Figures S2 and S6).^{29–31} This can be directly verified by the HRTEM images in Figure 1D and Figure S7. The strong multiple hydrogen-bonding networks of CMN nanosheets exhibit clear lattice structure, while *g*-C₃N₄ nanosheets display typical triazine unit structure. Moreover, the *d* values of lattice spacing are 0.299 and 0.324 nm, matching well with the spacing of the (002) crystal planes of CMN and *g*-C₃N₄ nanosheets, respectively (Figure S8).^{19,31} Furthermore, EDS mappings (Figure 1C; Figure S9) reveal that C and N elements are evenly distributed on nanosheet

surface, while O element that only belongs to CMN appears clumped distribution, confirming the alternate structure of CM/C₃N₄ nanosheet.

3.2 | Morphologies and microstructures of lamellar membranes

Next, the nanosheets were uniformly dispersed in IPA and then slowly stacked on Nylon substrate through vacuum filtration to assemble lamellar membranes (Figure S10). Slow filtration procedure ensures the ordered stacking of nanosheets, forming straight and regular interlayer channels in membrane.^{36,37} This is identified by the smooth membrane surface and ordered layer-by-layer stacking of nanosheets in cross-sectional SEM images (Figure 2A,B; Figures S11–S13). The ordered stacking of nanosheets brings a sharp (002) peak at $2\theta = 6.7^\circ$ in XRD patterns (Figure 2C), corresponding to close interlayer spacing of ~1.3 nm for these lamellar membranes.^{38,39} Specifically, hydrophobic *g*-C₃N₄ membrane shows an interlayer spacing of 1.27 nm, while the abundant hydroxyl and carbonyl groups on CMN and CM/C₃N₄ nanosheets exhibit slightly larger interlayer spacings of 1.32 and 1.33 nm, respectively, for lamellar membranes. This can be further verified by the N₂ adsorption-desorption isotherms and pore-size distribution (Figure S14). The *g*-C₃N₄ membrane displays a pore diameter of 1.17 nm and pore volume of 0.28 cm³ g⁻¹, which are close to, but slightly lower than those of CMN (1.23 nm and 0.31 cm³ g⁻¹) and CM/C₃N₄ (1.21 nm and 0.29 cm³ g⁻¹) membranes. Here, membrane

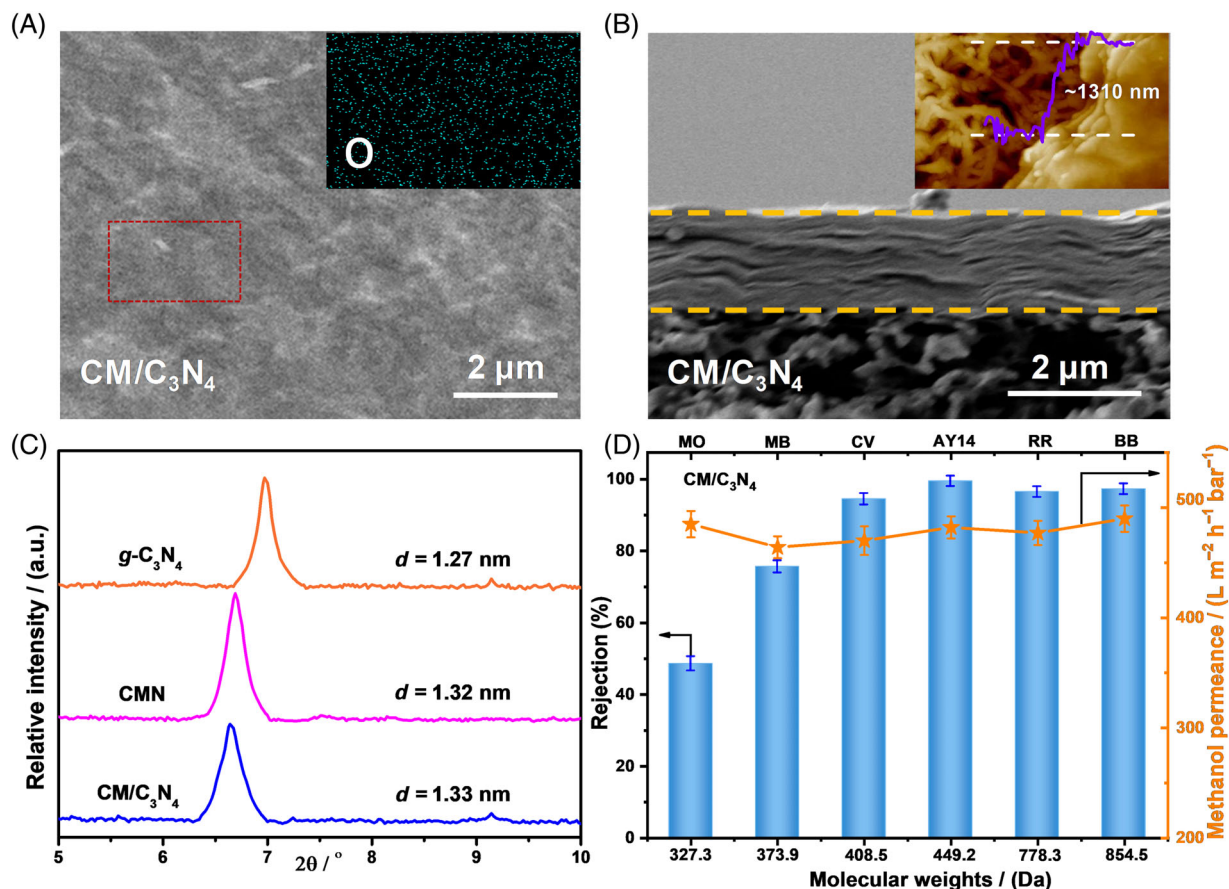


FIGURE 2 Characterization for the microstructures of lamellar membranes. (A) Surface scanning electron microscopy (SEM) image of heterostructured CM/C₃N₄ membrane (inset: elemental mapping of O). (B) Cross-sectional SEM image of heterostructured CM/C₃N₄ membrane (inset: cross-sectional atomic force microscopy image and the corresponding height profile). (C) X-ray diffraction patterns of membranes in solvated state. (D) Dye rejection with the variation of molecular weights (left axis) and the corresponding methanol permeance (right axis) for heterostructured CM/C₃N₄ membrane

thickness can be controlled by nanosheet loading (Figure S15), and a thickness of around 1310 nm is adopted for favorable structural stability.

The highly regular, similar channels of lamellar membranes are further supported by the precise rejection for dyes (Figure 2D). Here, six common industrial dyes with distinct sizes and charges were dispersed in methanol and separated through the membranes (Table S1 and Figure S16). Before the rejection test of lamellar membrane, the membranes were immersed in various dye solutions for 3 h and the UV-vis absorption spectra of dye solutions before and after immersion were measured (Figure S17). It shows that the variation of maximum absorbance value of dye solutions is less than 5%, suggesting that the effect of dye adsorption on membrane rejection is limited, and the rejection of dyes is mainly based on size sieving mechanism.^{16,40} It shows that the rejection of all membranes for methylene blue with size of 1.2 nm is only ~75%, while it lifts to over 90% when dye size increases to 1.5 nm (CV). Further increasing dye size to 1.9 nm (acid yellow14) elevates the rejection to nearly 100% (Figures S18 and S19). And these lamellar membranes meanwhile exhibit high methanol permeance of over 200 L m⁻² h⁻¹ bar⁻¹, which

is benefited from the regular nanochannels that permit continuous flow of small solvents. These imply that the channel size lies between 1.2 and 1.5 nm, and the close rejection results indicate that all membranes possess similar interlayer channels. Note that CM/C₃N₄ membrane with weak negative property gives slightly higher rejection for negatively charged RosB (78.5%) than that for positively charged MB (74.6%). This indicates that the electrostatic repulsion between membrane and dyes influences membrane rejection to a certain degree, while the impact is limited.⁴¹

3.3 | Wettability and solvent uptake of lamellar membranes

These membranes display different wettability as confirmed by the time-dependent water contact angles because of the distinct chemical components. Figure 3A shows that g-C₃N₄ membrane gives high water contact angle of over 93° for 20 s, confirming the hydrophobic character of g-C₃N₄ nanosheets.²⁸ While the water contact angle substantially reduces from 43° to 4° over 20 s for CMN membrane,

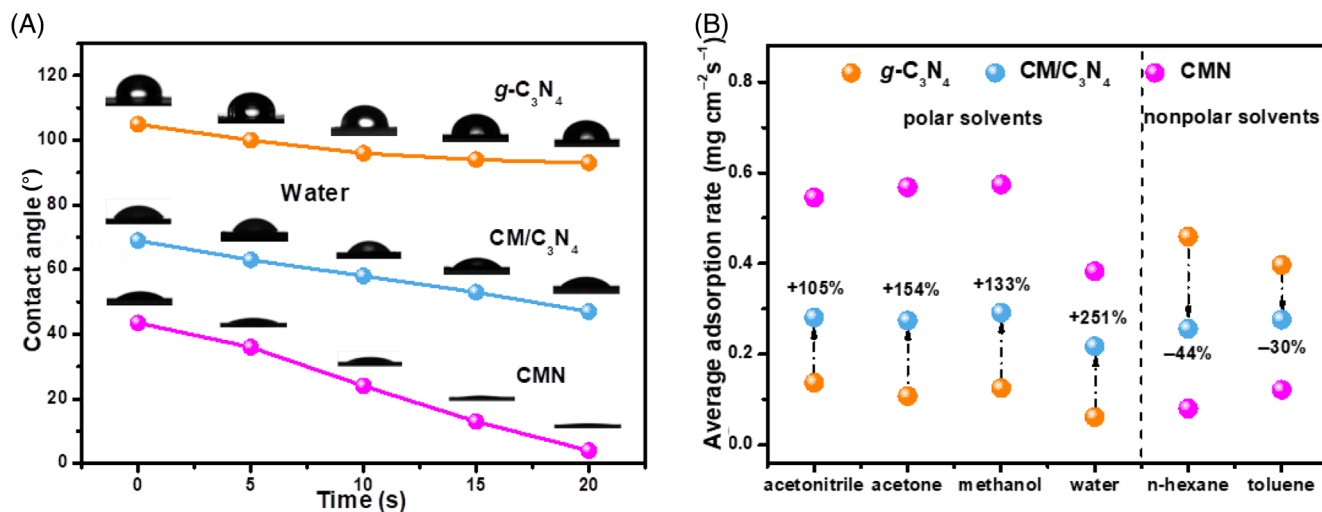


FIGURE 3 Proofs for the hydrophilicity and hydrophobicity of lamellar membrane. (A) Water contact angles and (B) average adsorption rates of membranes

highlighting the hydrophilic feature of CMN nanosheets. Interestingly, CM/C₃N₄ membrane exhibits moderate reduction of water contact angle from 69° to 47° within 20 s because of the amphipathic property of CM/C₃N₄ nanosheets. Moreover, this further brings distinct dissolution ability for lamellar membranes to polar and nonpolar solvents, as verified by the average adsorption rate of solvents (Figure 3B; Note S3). Hydrophilic CMN membrane acquires the highest adsorption rate for polar solvents but the lowest value for nonpolar ones. As examples, acetonitrile and acetone acquire the average adsorption rates of 0.54 and 0.57 mg cm⁻² s⁻¹, respectively, while those of n-hexane and toluene are only 0.08 and 0.12 mg cm⁻² s⁻¹, respectively. In contrast, hydrophobic g-C₃N₄ membrane gives favorable adsorption for nonpolar solvents but poor adsorption for polar ones. Considering that the interlayer space of these membranes is similar, that is comparable storage spacing, the discrepant adsorption rate should originate from the diverse dissolution ability to molecules. These indicate that hydrophilic CMN membrane has strong dissolution to polar solvents while repels nonpolar ones, and the condition is inverse for hydrophobic g-C₃N₄ membrane. Whereas heterostructured CM/C₃N₄ membrane exhibits comparable affinity and hence dissolution ability for polar and nonpolar solvents. For instance, the average adsorption rates for acetonitrile and n-hexane are 0.28 and 0.26 mg cm⁻² s⁻¹, respectively. This further indicates the parallel opportunities to enter channels for further diffusion.

3.4 | Correlation between solvent permeation and dissolution-diffusion

Next, the molecule transfer properties of lamellar membranes were evaluated under pressure of 1 bar by a home-made device after being measured for 3 h to ensure a stable permeance (Figure S20). Note that the treated Nylon support exhibits ultrafast molecule permeance (more than 4000 L m⁻² h⁻¹ bar⁻¹ for water), yet negligible rejection

for dyes (below 20%) (Figures S21 and S22).¹³ Results show that the lamellar membranes acquire high molecule permeance. The permeances of acetonitrile and acetone reach 1025 and 953 L m⁻² h⁻¹ bar⁻¹ for CM/C₃N₄ membrane, respectively, which are outstanding as compared with polymer and most reported lamellar membranes (Figure 4A; Figure S23). This is attributed to the regular channels that allow continuous and steady molecular-flow with low resistance.^{15,42} Here, hydrophobic g-C₃N₄ membrane displays excellent permeation for nonpolar solvents as compared to polar ones (Figure S24). For instance, the permeances for n-hexane and toluene are 451 and 354 L m⁻² h⁻¹ bar⁻¹, while those of water and acetone are 188 and 317 L m⁻² h⁻¹ bar⁻¹, respectively. In contrast, hydrophilic CMN membrane gives higher permeances for polar solvents but lower values for nonpolar ones. The permeances for acetone and n-hexane are 504 and 166 L m⁻² h⁻¹ bar⁻¹, respectively. Additionally, considering the practical application of membranes, dyes were dissolved in solvents for the measurement of nanofiltration performance. Results in Figure S25a reveal that in the presence of dyes, solvent permeance is generally decreased by ~10% as compared to the corresponding pure solvent. This should be ascribed to the slight fouling of membrane surface by dyes.^{43,44}

Molecules transfer through lamellar membrane should firstly dissolve on membrane surface and then diffuse in inner channels.^{1,42,45} The favorable dissolution abilities of hydrophilic CMN membrane to polar solvents and hydrophobic g-C₃N₄ membrane to nonpolar solvents help to achieve their high permeation. Figure 4B and Figure S25b show that, as compared to hydrophobic g-C₃N₄ membrane, introducing hydrophilic nanodomains on CM/C₃N₄ membrane surface permits more than 120% permeance increment for polar solvents. Analogously, the presence of hydrophobic nanodomains on CM/C₃N₄ membrane surface brings substantially elevated permeance for nonpolar solvents as compared to CMN membrane. These findings confirm that for lamellar membranes with distinct wettability, the transfer discrepancy for both polar and nonpolar solvents is affected

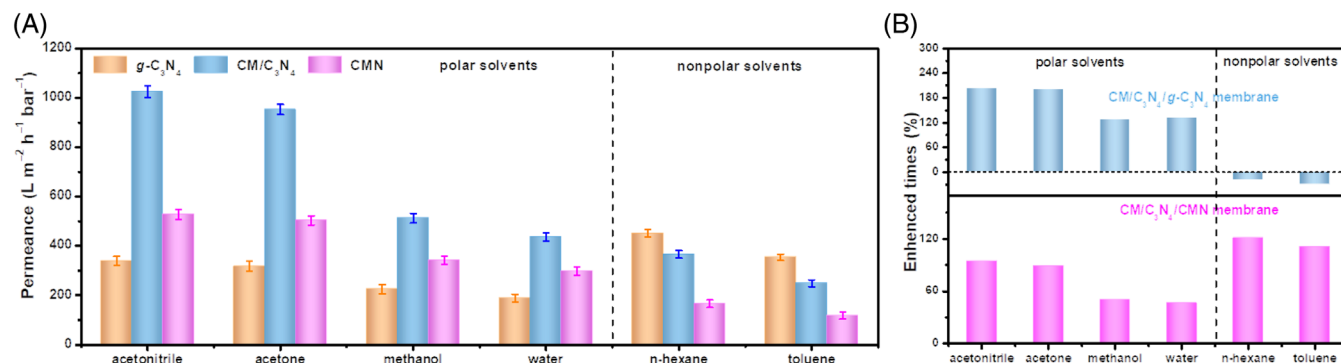


FIGURE 4 (A) Solvent permeance of the membranes. (B) The upper is the enhanced times of solvent permeance for heterostructured CM/C₃N₄ to hydrophobic g-C₃N₄ membranes and the bottom is that for heterostructured CM/C₃N₄ to hydrophilic cyanuric acid melamine membranes.

by the dissolution process on membrane surface. In addition, it shows that heterostructured CM/C₃N₄ membrane, which possesses comparable solvent dissolution ability, exhibits much higher permeance for polar solvents than that for nonpolar ones. For example, acetonitrile receives a high permeance of 1025 L m⁻² h⁻¹ bar⁻¹, while that of n-hexane is 366 L m⁻² h⁻¹ bar⁻¹, indicating that diffusion process in inner channels plays distinct role on the transfer of polar and nonpolar solvents. In comparison with CMN membrane, the existence of hydrophobic nanodomains on CM/C₃N₄ membrane, in contrast, gives more than 45% improvement for polar solvents. Considering the depressed dissolution of polar solvents on CM/C₃N₄ membrane surface, the abnormally elevated permeance should result from fast molecule diffusion in inner channels. While nonpolar solvents do not display such specificity. Therefore, for lamellar membranes with distinct wettability, the transfer discrepancy of polar solvents should be originated from both dissolution and diffusion processes.

3.5 | Theoretical analysis of correlations

To confirm this hypothesis, the solid-liquid interface interaction free energy (γ_{SL}) and diffusion coefficient (D) are calculated via Young's equation (3) and Fick's law (5), respectively (Notes S1 and S2).^{21,46}

$$\gamma_S - \gamma_{SL} = \gamma_L \cdot \cos\theta, \quad (3)$$

where γ_S , γ_L , γ_{SL} , and θ represent the solid surface energy, liquid surface energy, solid-liquid interface interaction free energy, and contact angle, respectively. The relationship between γ_S , γ_L , and θ can be expressed as:

$$\cos\theta = -1 + 2 \cdot \sqrt{\frac{\gamma_S}{\gamma_L}} \cdot e^{[-\beta(\gamma_S - \gamma_L)^2]}, \quad (4)$$

where $\beta = 0.000125 \text{ (m}^2 \text{ MJ}^{-1})^{-2}$.

$$J = -D \cdot \frac{dC}{dx}. \quad (5)$$

In Equation (5), the D , dC , dx represent the solvent diffusion coefficient (m² s⁻¹) in the membrane, concentration difference, diffusion distance (m), respectively. The γ_{SL} results reveal that CMN and CM/C₃N₄ membranes give much lower γ_{SL} values for polar solvents, as compared to g-C₃N₄ membrane (Figure 5A). This fact indicates that CMN and CM/C₃N₄ membranes have strong dissolution ability for polar solvents, while g-C₃N₄ membrane displays poor dissolution for polar solvents. While the condition is just inverse for nonpolar solvents, which exhibit well dissolution with g-C₃N₄ and CM/C₃N₄ membranes but barren dissolution with CMN membrane. These observations match well with the discrepant solvent permeance. This phenomenon demonstrates that the permeance difference of both polar and nonpolar solvents is affected by the dissolution process on membrane surface. For another, Figure 5B reveals that the D values of polar solvents in three kinds of lamellar membrane channels obey the order of CM/C₃N₄ > CMN > g-C₃N₄. While for nonpolar solvents, the D values are much lower and comparable in these membrane channels. These phenomena collectively confirm that for lamellar membranes with close physical structure but distinct wettability, the transfer discrepancy of polar solvents is stemmed from both dissolution and diffusion processes, while that of nonpolar solvents is mainly originated from diffusion process. Note that water molecules possess abnormally high γ_{SL} values for these lamellar membranes. This should be ascribed to the unrivaled surface tension of water, giving weaker dissolution on membrane surface than that of other polar solvents.⁴⁷

Next, the parameters of D and γ_{SL} are utilized to quantitatively describe molecule transfer behavior in lamellar membranes. As expected, a transport model that well correlates permeance (P_s) of a polar solvent s and the parameters is proposed for CM/C₃N₄ membrane (Figure 5C). The equation can be expressed as:

$$P_s = A \cdot D \cdot \gamma_{SL}^{-1/2}, \quad (6)$$

where A is a proportionality constant (mJ^{-1/2} m⁻² bar⁻¹). Note that the basic physical parameters of membrane (pore size, thickness, surface porosity, etc.) are fixed for a certain membrane, and these parameters are included in the proportionality constant A of the equations.^{15,48} Note that the equation proposed herein is similar to

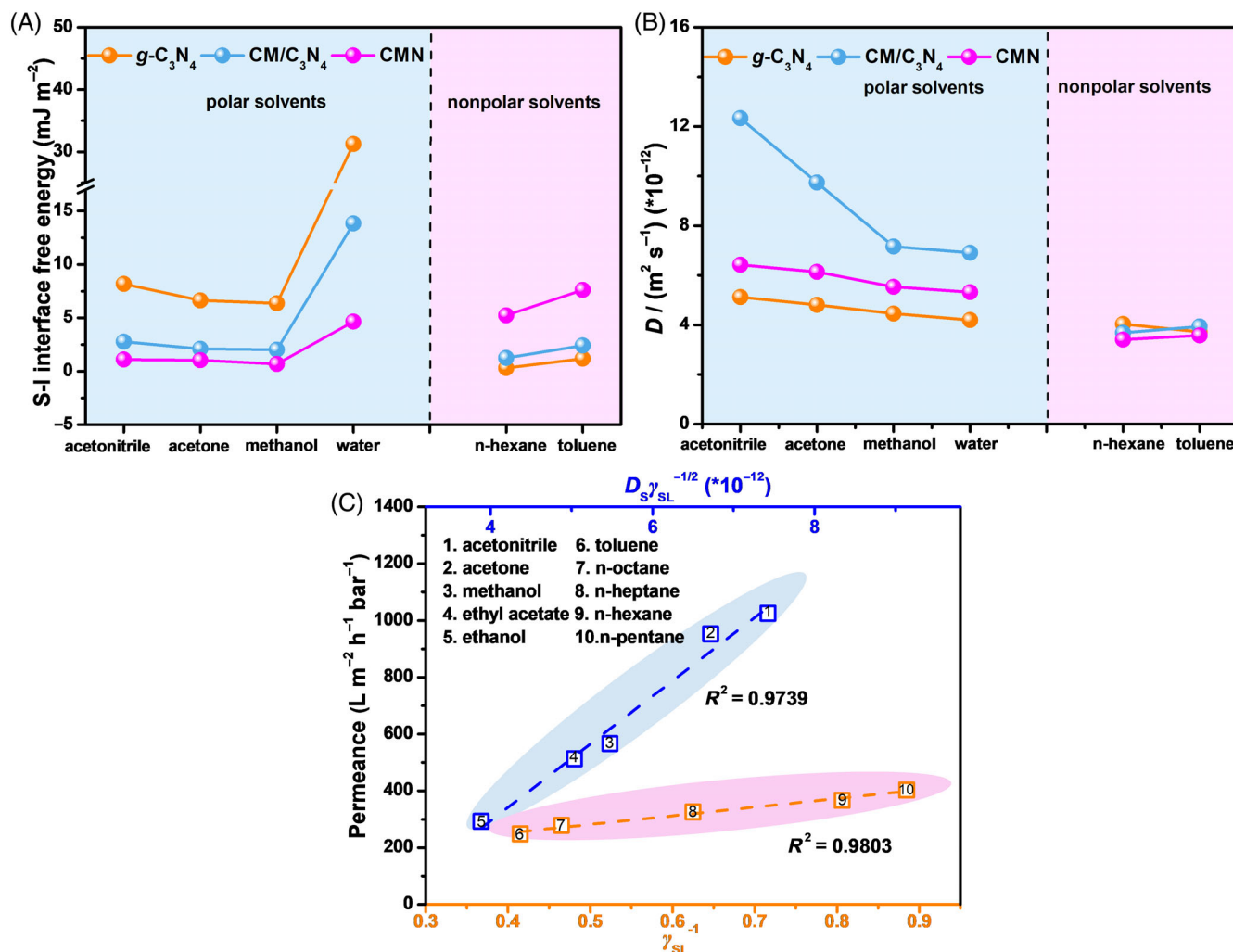


FIGURE 5 (A) Solid-liquid interface interaction free energy and (B) diffusion coefficient comparison for membranes. (C) The upper is polar solvent permeance against the γ_{SL} and D , and the bottom is the nonpolar solvent permeance against for the γ_{SL} for heterostructured CM/C₃N₄ membrane.

the one for describing the uncharged organics transport through polymer membranes with uniform free-volume paths:

$$J_s = \frac{\Delta C \cdot (1 - \lambda)^2}{\Delta x} \cdot \frac{D_s}{\sqrt{kT/e^{\gamma_{SL}}}}, \quad (7)$$

where $\lambda = r_s/r_p$ is the ratio of solute radius (r_s) to the hypothetical membrane pore radius (r_p), k and T represent the Boltzmann constant (m² kg s⁻² K⁻¹), the absolute temperature (K), respectively. This equation verifies that the transfer discrepancy of polar solvents is originated from both dissolution and diffusion processes. While the permeances of nonpolar solvents show a relationship as follow:

$$P_s = A' \cdot \gamma_{SL}^{-1}, \quad (8)$$

where A' is a proportionality constant (mJ m⁻¹ h⁻¹ bar⁻¹). The proportional $P_s - \gamma_{SL}^{-1/2}$ relation for polar solvents turns to a $P_s - \gamma_{SL}^{-1}$

relation for nonpolar ones. This may be ascribed to the weak nonpolar intermolecular interactions, leading to a more significant effect of γ_{SL} .^{49,50} This reveals that the transfer discrepancy of nonpolar solvents is mainly stemmed from dissolution process due to weak channel-molecule interactions. These two equations clearly verify the distinct transfer behaviors of polar and nonpolar solvents, and more importantly, they give new viewpoint in transfer mechanism of lamellar membrane.⁵¹⁻⁵³ Besides, by adjusting the CM/C₃N₄ membrane thickness from 960 to 1850 nm, the calculated D values for acetone are comparable with variation below 5%, and the variation of D values for hexane is also below 5% (Figure S26). Moreover, this condition is also found for CMN and g-C₃N₄ membranes, confirming that conclusion should be applicative for other lamellar membranes with different thicknesses. In addition, by adjusting the testing pressure from 1 to 3 bar, the calculated D values are also comparable with variation below 5% (Figure S27). This observation implies that the conclusion should be applicative in different testing conditions. Note that the

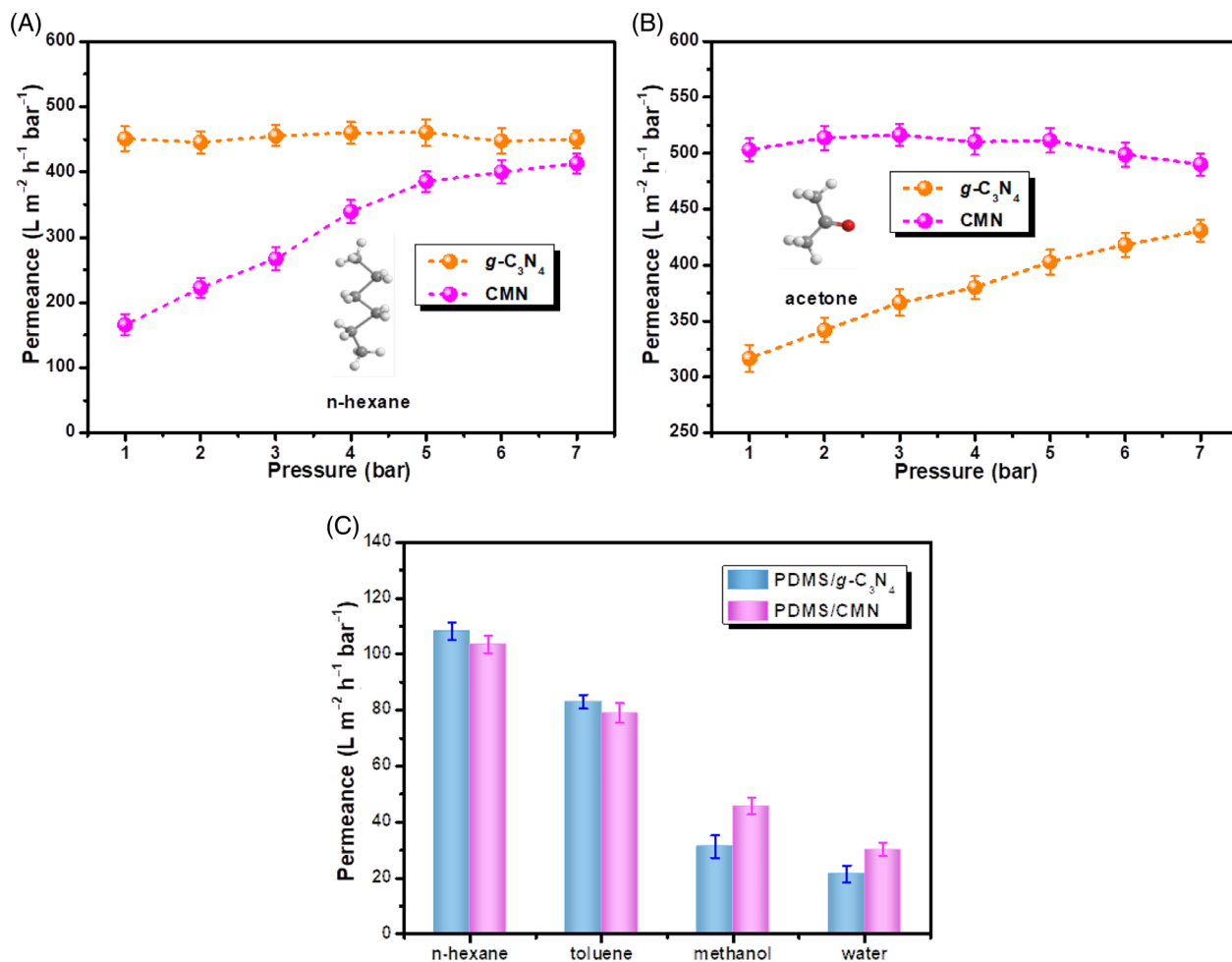


FIGURE 6 Permeance of (A) n-hexane and (B) acetone as a function of transmembrane pressure for hydrophobic $g\text{-C}_3\text{N}_4$ and hydrophilic cyanuric acid melamine (CMN) membranes. (C) Solvent permeance of polydimethylsiloxane (PDMS)/ $g\text{-C}_3\text{N}_4$ and PDMS/CMN membranes

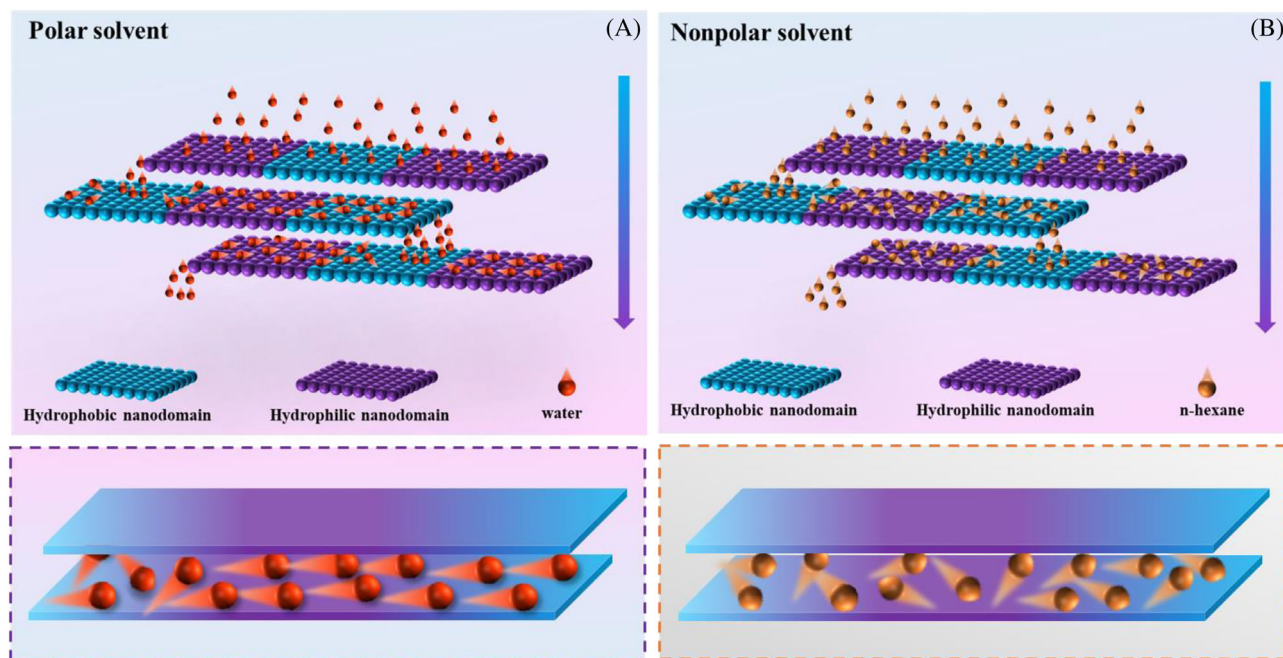


FIGURE 7 Schematic diagrams of (A) polar solvent molecules and (B) nonpolar solvent molecules transfer from the upper layer to the lower layer in heterostructured CM/ C_3N_4 membrane

above equations can only be established by heterostructured membranes, while single hydrophilic or hydrophobic membrane fails to do so. This is mainly because that, the heterostructured membrane allows comparable surface affinity for diverse molecules. It can avoid molecule insolubility on membrane surface, thus confounding the effect of diffusion for transfer.

3.6 | The effect of dissolution and diffusion on solvent permeation

Based on the above transfer mechanism, pressure-dependent molecule permeance was measured as shown in Figure 6A,B. Figure 6A reveals that the permeance of n-hexane increases obviously from 167 to $386 \text{ L m}^{-2} \text{ h}^{-1} \text{ bar}^{-1}$ as pressure elevates from 1.0 to 5.0 bar for CMN membrane. While the permeance of n-hexane maintains at around $445 \text{ L m}^{-2} \text{ h}^{-1} \text{ bar}^{-1}$ for hydrophobic $g\text{-C}_3\text{N}_4$ membrane. This

suggests that pressure acts as driving force for nonpolar solvent to enter into hydrophilic CMN membrane channels, while hydrophobic $g\text{-C}_3\text{N}_4$ membrane can directly dissolve them into inner channels.^{16,54} After over dissolution enthalpy, n-hexane obtains similar diffusion property in both hydrophilic and hydrophobic channels, as supported by the comparable permeances under pressure of 7.0 bar. Likely, pressure also helps polar solvents to enter hydrophobic channels when taking acetone as an example. Differently, acetone permeance in CMN membrane is always higher than that in $g\text{-C}_3\text{N}_4$ membrane, even overcoming the dissolution enthalpy. This further verifies the significant effect of diffusion process on the transfer of polar solvents (Figure 6B). For a direct comparison, a thin polymer layer of hydrophobic PDMS was sprayed on the surface of CMN and $g\text{-C}_3\text{N}_4$ membranes, which were donated as PDMS/CMN and PDMS/ $g\text{-C}_3\text{N}_4$, respectively (Figure 6C; Figure S28). In this manner, they possess strong and similar dissolution ability toward solvent molecules. Results show that PDMS/CMN and PDMS/ $g\text{-C}_3\text{N}_4$ membranes display

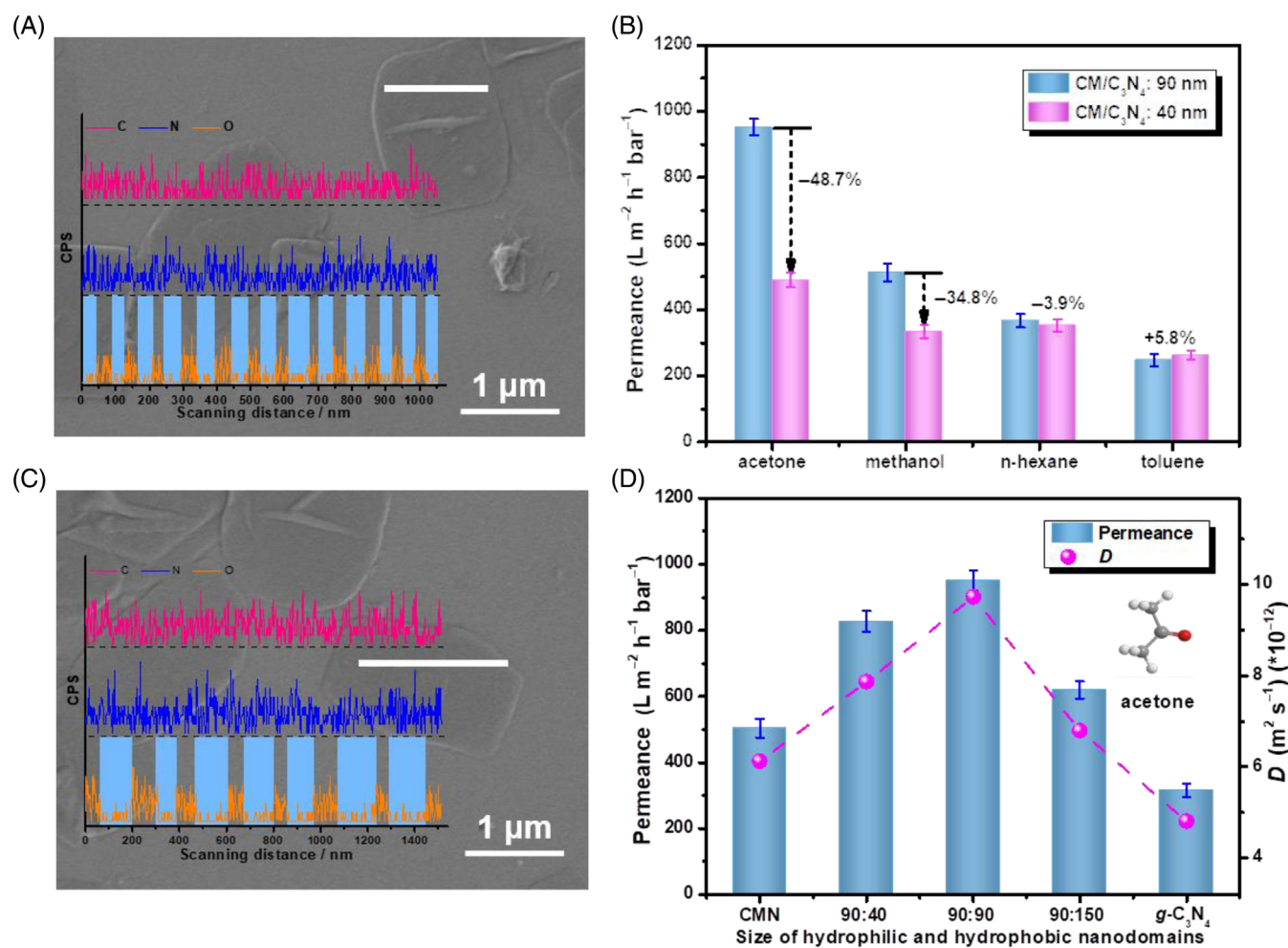


FIGURE 8 (A) Scanning electron microscopy (SEM) image of heterostructured CM/C₃N₄ nanosheet with hydrophilic and hydrophobic nanodomain size of about 40 nm (inset: elemental line scanning of C, N, and O). (B) Permeance comparison for heterostructured CM/C₃N₄ membrane prepared by heterostructured nanosheets with varied size of hydrophilic and hydrophobic nanodomains. (C) SEM image of heterostructured CM/C₃N₄ nanosheet with hydrophilic and hydrophobic nanodomains of about 90 and 150 nm, respectively (inset: elemental line scanning of C, N, and O). (D) Permeance and corresponding *D* comparison for heterostructured CM/C₃N₄ membrane prepared by heterostructured nanosheets with varied size of hydrophilic and hydrophobic nanodomains

comparable permeance for nonpolar solvents, confirming the similar effect of diffusion process on their transfer ability. As for polar solvents, hydrophilic channels within PDMS/ $g\text{-C}_3\text{N}_4$ membrane permit higher permeance than PDMS/CMN membrane with hydrophobic channels. This is ascribed to the hydrophilic channels that afford faster diffusion rate for polar solvents.

The preliminary results show that heterostructured CM/ C_3N_4 membrane achieves higher permeance for polar solvents as compared to hydrophilic CMN membrane. For instance, the permeances for acetonitrile and acetone reach 1025 and $953 \text{ L m}^{-2} \text{ h}^{-1} \text{ bar}^{-1}$, respectively, which are more than 1.8 times that of CMN membrane. Considering the depressed dissolution ability of CM/ C_3N_4 membrane for polar solvents, the boosted permeance should be originated from the enhanced diffusion ability in channels. Previous studies have demonstrated that molecular configuration significantly affects its diffusion in confined nanochannels.^{21,55–58} Presumably, the hydrophilic nanodomains drive polar solvents to form orderly aligned aggregates

along channel walls through hydrogen-bonding interactions, which permits fast diffusion (Figure 7A). Then, this aligned aggregate state is maintained when passing into the adjacent hydrophobic nanodomains, and the smooth $g\text{-C}_3\text{N}_4$ boundary allows a slip by low-friction movement.^{19,59} This novel synergistic process contributes to the fast diffusion (i.e., high D value) in heterostructured channels.

This can be further explored by tuning the respect lateral length of single CMN and $g\text{-C}_3\text{N}_4$ nanosheets, corresponding to length and ratio of hydrophilic and hydrophobic nanodomains in channels, respectively. Here, the total nanosheet size and membrane thickness are controlled to be comparable. Figure 8A,B reveals that when the lateral lengths of hydrophilic and hydrophobic nanodomains reduce from ~ 90 to ~ 40 nm, the permeance of polar solvents decreases significantly (about 50%), while that of nonpolar solvents shows much less change (about 6%). This should be originated from the fact that hydrophilic nanodomains are too short to fully induce the ordered aggregation of polar solvents. Then, the lateral length of hydrophobic

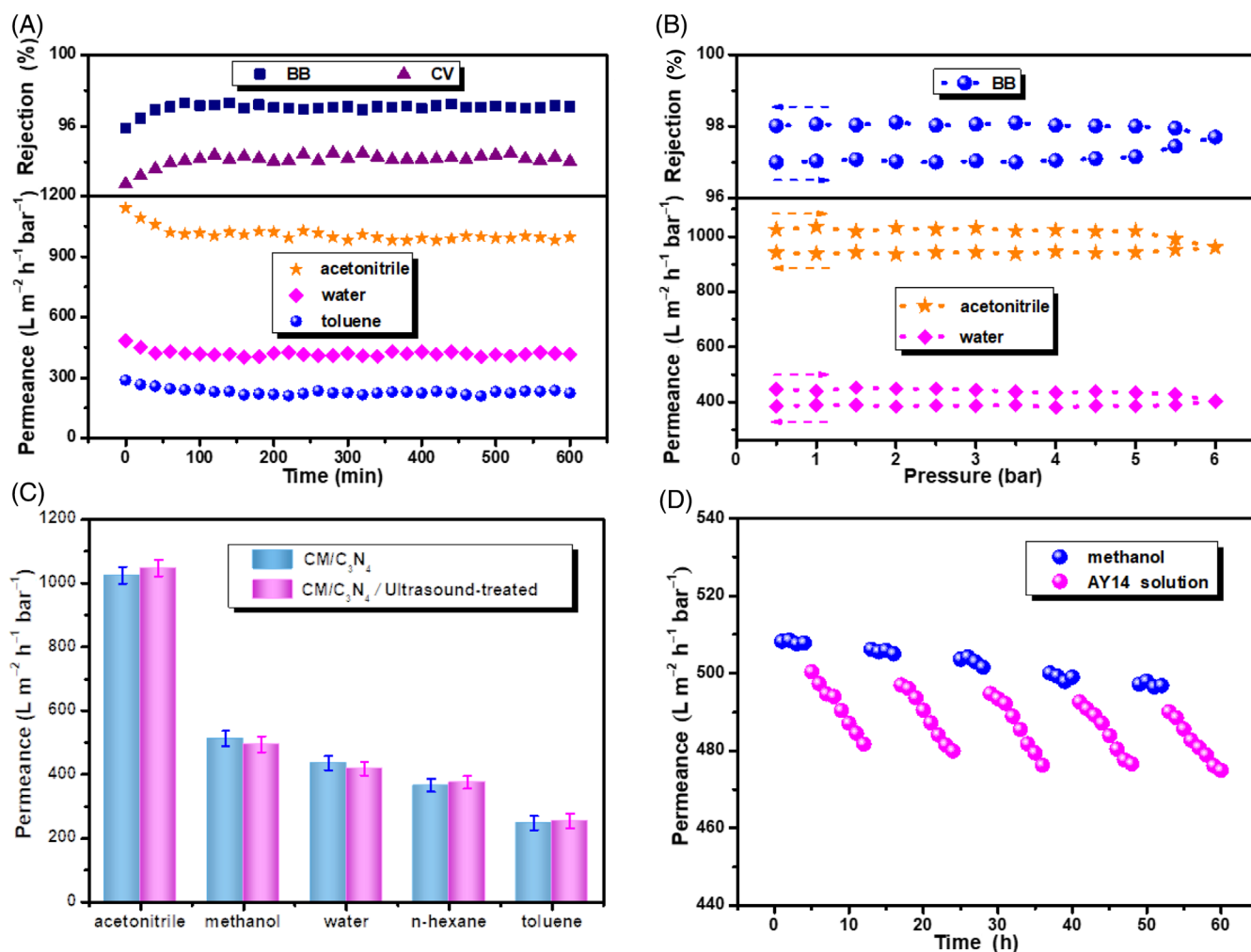


FIGURE 9 Proofs for the stability of heterostructured CM/ C_3N_4 membrane. (A) Long-term operation performance of CM/ C_3N_4 membrane in the permeance of acetonitrile, water, and toluene and rejection of BB and CV under 1 bar. (B) The variation of permeance and rejection of CM/ C_3N_4 membrane with transmembrane pressure. (C) Solvent permeance of CM/ C_3N_4 membrane before and after ultrasound treatment for 10 min. (D) Demonstration of the low-fouling behavior of CM/ C_3N_4 membrane during filtration of an AY14 solution (0.1 g L^{-1}) and permeance recovery after water cleaning in five cycles

nanodomain was manipulated while maintaining that of hydrophilic nanodomain at ~90 nm. We find that the acetone permeance drops when ulteriorly boosting the lateral size of hydrophobic nanodomains from ~90 to ~150 nm (Figure 8C,D). And the corresponding D values also experience a reduction from 9.7×10^{-12} to $6.8 \times 10^{-12} \text{ m}^2 \text{ s}^{-1}$, since the prolonged hydrophobic nanodomain is too long to maintain the ordered molecule aggregation.^{57,60} These phenomena highlight the decisive contribution of the synergistic process to fast diffusion in heterostructured channels, matching well with the Arrhenius activation energy of water conduction through membranes (Figure S29).^{22,28,61} In contrast, as for nonpolar solvents (Figure 7B), the weak interactions between channel walls and solvents make them keep disordered distribution state in channels, which would result in random collision among molecules and even collide with channel walls.¹⁵ Thus, a relatively slower transfer occurs resulting from the impaired velocity of molecules as compared with polar solvents.

3.7 | Operation stability of lamellar membranes

The structural stability of CM/C₃N₄ membrane was evaluated, which shows that the membrane gives relatively stable performance during a continuous 600 min operation (Figure 9A). It should be noted that there is a slight permeance decrease and rejection increase in the initial 120 min, and the variation rate is below $0.02\% \text{ min}^{-1}$. This is originated from sheet compaction within laminate structure and slight adsorption of dyes on membrane surface, which restrict the transfer of molecules. While the membrane can keep a high and stable performance in the following time (Figure S30a). And the robust stacking structure also provides favorable pressure resistance for CM/C₃N₄ membrane, which bears the pressure as high as 5.0 bar without structural collapse. Further increasing the pressure to 6.0 bar brings a variation below 5% in molecule permeance and dye rejection (Figure 9B; Table S3 and Figure S30b). Moreover, the intact stacking structure can be maintained even soaking in HCl solution for more than 20 min or under ultrasound for 10 min (Figure 9C; Figure S31). Additionally, the heterostructured and smooth surface of CM/C₃N₄ membrane also offers outstanding antifouling capability and washing durability. This is benefited from the water molecule layers on membranes surface, which restrict the adhesion of pollutants (Figure 9D; Note S4).^{16,62}

4 | CONCLUSIONS

In summary, heterostructured nanosheets assembled by small-sized hydrophilic CMN and hydrophobic $g\text{-C}_3\text{N}_4$ nanosheets were designed as building blocks to prepare lamellar membranes. Based on this heterostructured platform, we demonstrate that polar and nonpolar solvents show distinct molecule transfer mechanism. For lamellar membranes with distinct wettability, the transfer discrepancy of polar solvents is originated from both dissolution and diffusion processes, while that of nonpolar solvents is mainly stemmed from dissolution process. Accordingly, the corresponding equations which are suitable

for heterostructured lamellar membranes are established. Furthermore, we demonstrate that polar solvents are induced to form orderly aligned arrangement along channel walls in hydrophilic nanodomains and then maintain this ordered state in adjacent hydrophilic nanodomains. This permits fast diffusion with low resistance, giving high polar solvent permeance of $1025 \text{ L m}^{-2} \text{ h}^{-1} \text{ bar}^{-1}$ for acetonitrile. Moreover, regulating the lateral length and ratio of hydrophilic and hydrophobic nanodomains can manipulate molecule diffusion in heterostructured channels. In contrast, nonpolar solvents with disordered arrangement display comparable diffusion property in both polar and nonpolar channels, but the permeance is lower than that of polar solvents. This elaboration of molecule transfer mechanism in lamellar membranes can provide valuable guidance for rational design of high-efficient separation membranes. Furthermore, the polar solvent permeance varies distinctly with the length ration of hydrophilic and hydrophobic nanodomains within channels, and the channels with length of ~90 nm:90 nm exhibit the highest permeance. Besides, the heterostructured membrane gives high and stable performance for more than 36 h, confirming the excellent structural stability. These findings demonstrate that this novel membrane holds potential for practical industrial applications.

NOMENCLATURE

Abbreviations

$g\text{-C}_3\text{N}_4$	graphitic carbon nitride
CMN	cyanuric acid melamine
CM/C ₃ N ₄	cyanuric acid melamine/graphitic carbon nitride
PDMS/CMN	the thin PDMS layer on CMN membrane surface
PDMS/ $g\text{-C}_3\text{N}_4$	the thin PDMS layer on $g\text{-C}_3\text{N}_4$ membrane surface

Symbols

γ_s	the solid surface energy (mJ m^{-2})
γ_{SL}	the solid-liquid interface interaction free energy (mJ m^{-2})
γ_L	the liquid surface energy (mJ m^{-2})
D	diffusion coefficient ($\text{m}^2 \text{ s}^{-1}$)
k	the Boltzmann constant ($\text{m}^2 \text{ kg s}^{-2} \text{ K}^{-1}$)
T	the absolute temperature (K)
P_s	solvent permeance ($\text{L m}^{-2} \text{ h}^{-1} \text{ bar}^{-1}$)
ΔP	operating pressure (bar)
V_p	permeate volume (L)
C_p	the concentration of permeate side solution (g L^{-1})
C_f	the concentration of feed solution (g L^{-1})
A	effective membrane area (m^2)
t	testing time (h)
R	rejection (%)

AUTHOR CONTRIBUTIONS

Chongchong Chen: Data curation (equal); investigation (equal); writing – original draft (equal); writing – review and editing (equal). **Xiaoli Wu:** Data curation (equal); investigation (equal); software (equal); writing – original draft (equal); writing – review and editing (equal). **Jie Zhang:** Data curation (equal); investigation (equal). **Jingjing Chen:** Software (equal); writing – original draft (equal). **Xulin Cui:** Investigation (equal);

software (equal). **Wenpeng Li**: Supervision (equal); writing – original draft (equal). **Wenjia Wu**: Project administration (equal); supervision (equal). **Jingtao Wang**: Funding acquisition (equal); project administration (equal); supervision (equal); writing – original draft (equal); writing – review and editing (equal).

ACKNOWLEDGMENTS

The authors gratefully acknowledge the financial support from the National Natural Science Foundation of China (No. U2004199), the Natural Science Foundation of Henan Province (212300410285), and the Henan Natural Science Funds for Excellent Young Scholar (202300410373). The Center for Advanced Analysis and Computational Science, Zhengzhou University is also gratefully acknowledged.

DATA AVAILABILITY STATEMENT

The data that support the findings of this study are available from the corresponding author upon reasonable request.

ORCID

Jingtao Wang  <https://orcid.org/0000-0002-2004-9640>

REFERENCES

- Liu G, Jin W, Xu N. Two-dimensional-material membranes: a new family of high-performance separation membranes. *Angew Chem Int Ed*. 2016;55:13384-13397.
- Ding L, Wei Y, Li L, et al. MXene molecular sieving membranes for highly efficient gas separation. *Nat Commun*. 2018;9:155.
- Zhou KG, Vasu KS, Cherian CT, et al. Electrically controlled water permeation through graphene oxide membranes. *Nature*. 2018;559:236-240.
- Huang L, Chen J, Gao T, et al. Reduced graphene oxide membranes for ultrafast organic solvent nanofiltration. *Adv Mater*. 2016;28:8669-8674.
- Ding L, Wei Y, Wang Y, Chen H, Caro J, Wang H. A two-dimensional lamellar membrane: MXene nanosheet stacks. *Angew Chem Int Ed*. 2017;129:1-6.
- Culp TE, Khara B, Brickey KP, et al. Nanoscale control of internal inhomogeneity enhances water transport in desalination membranes. *Science*. 2021;371:72-75.
- Echaide-Górriz C, Malankowska M, Téllez C, Coronas J. Nanofiltration thin-film composite membrane on either the internal or the external surface of a polysulfone hollow fiber. *AIChE J*. 2020;66:e16970.
- Huang K, Liu G, Shen J, et al. High-efficiency water-transport channels using the synergistic effect of a hydrophilic polymer and graphene oxide laminates. *Adv Funct Mater*. 2015;25:5809-5815.
- Wang Y, Liu L, Xue J, Hou J, Ding L, Wang H. Enhanced water flux through graphitic carbon nitride nanosheets membrane by incorporating polyacrylic acid. *AIChE J*. 2018;64:2181-2188.
- Zhang WH, Yin MJ, Zhao Q, et al. Graphene oxide membranes with stable porous structure for ultrafast water transport. *Nat Nanotechnol*. 2021;16:337-343.
- Lee CS, Choi M, Hwang YY, Kim H, Kim MK, Lee YJ. Facilitated water transport through graphene oxide membranes functionalized with aquaporin-mimicking peptides. *Adv Mater*. 2018;30:1705944.
- Karan S, Samitsu S, Peng X, Kurashima K, Ichinose I. Ultrafast viscous permeation of organic solvents through diamond-like carbon nanosheets. *Science*. 2012;335:444-447.
- Yang Q, Su Y, Chi C, et al. Ultrathin graphene-based membrane with precise molecular sieving and ultrafast solvent permeation. *Nat Mater*. 2017;16:1198-1202.
- Huang H, Song Z, Wei N, et al. Ultrafast viscous water flow through nanostrand-channelled graphene oxide membranes. *Nat Commun*. 2013;4:2979.
- Wang J, Chen P, Shi B, Guo W, Jaroniec M, Qiao SZ. A regularly channelled lamellar membrane for unparallelled water and organics permeation. *Angew Chem Int Ed*. 2018;57:6814-6818.
- Wang J, Yuan Z, Wu X, Li Y, Chen J, Jiang Z. Beetle-inspired assembly of heterostructured lamellar membranes with polymer cluster-patterned surface for enhanced molecular permeation. *Adv Funct Mater*. 2019;29:1900819.
- Liang F, Liu Q, Zhao J, et al. Ultrafast water-selective permeation through graphene oxide membrane with water transport promoters. *AIChE J*. 2020;66:e16812.
- Thebo KH, Qian X, Zhang Q, Chen L, Cheng HM, Ren W. Highly stable graphene-oxide-based membranes with superior permeability. *Nat Commun*. 2018;9:1486.
- Ran J, Pan T, Wu Y, et al. Endowing g-C₃N₄ membranes with superior permeability and stability by using acid spacers. *Angew Chem Int Ed*. 2019;58:1-8.
- Long Y, Wang K, Xiang G, Song K, Zhou G, Wang X. Molecule channels directed by cation-decorated graphene oxide nanosheets and their application as membrane reactors. *Adv Mater*. 2017;29:1606093.
- Wu X, Cui X, Wu W, Wang J, Li Y, Jiang Z. Elucidating the ultrafast molecular permeation through well-defined 2D nanochannels of lamellar membranes. *Angew Chem Int Ed*. 2019;58:18524-18529.
- Chen C, Wang J, Liu D, et al. Functionalized boron nitride membranes with ultrafast solvent transport performance for molecular separation. *Nat Commun*. 2018;9:1902.
- Wang Y, Gao B, Yue Q, Wang Z. Graphitic carbon nitride (g-C₃N₄)-based membranes for advanced separation. *J Mater Chem A*. 2020;8:19133-19155.
- Song Y, Li X, Fan JB, et al. Interfacially polymerized particles with heterostructured nanopores for glycopeptide separation. *Adv Mater*. 2018;30:1803299.
- Fu ZJ, Wang ZY, Liu ML, et al. Dual-layer membrane with hierarchical hydrophobicity and transport channels for nonpolar organic solvent nanofiltration. *AIChE J*. 2020;67:e17138.
- Meng X, Wang M, Heng L, Jiang L. Underwater mechanically robust oil-repellent materials: combining conflicting properties using a heterostructure. *Adv Mater*. 2018;30:1706634.
- Liu J, Hua D, Zhang Y, Japip S, Chung TS. Precise molecular sieving architectures with Janus pathways for both polar and nonpolar molecules. *Adv Mater*. 2018;30:1705933.
- Wu Y, Fu CF, Huang Q, et al. 2D heterostructured nanofluidic channels for enhanced desalination performance of graphene oxide membranes. *ACS Nano*. 2021;15:7586-7595.
- Zhang X, Xie X, Wang H, Zhang J, Pan B, Xi Y. Enhanced photo-responsive ultrathin graphitic-phase C₃N₄ nanosheets for bioimaging. *J Am Chem Soc*. 2013;135:18-21.
- Yang S, Gong Y, Zhang J, et al. Exfoliated graphitic carbon nitride nanosheets as efficient catalysts for hydrogen evolution under visible light. *Adv Mater*. 2013;25:2452-2456.
- Shalom M, Inal S, Fettkenhauer C, Neher D, Antonietti M. Improving carbon nitride photocatalysis by supramolecular preorganization of monomers. *J Am Chem Soc*. 2013;135:7118-7121.
- Hu M, Mi B. Enabling graphene oxide nanosheets as water separation membranes. *Environ Sci Technol*. 2013;47:3715-3723.
- Han Y, Xu Z, Gao C. Ultrathin graphene nanofiltration membrane for water purification. *Adv Funct Mater*. 2013;23:3693-3700.
- Zhang M, Mao Y, Liu G, Liu G, Fan Y, Jin W. Molecular bridges stabilize graphene oxide membranes in water. *Angew Chem Int Ed*. 2020;59:1689-1695.
- Shinde DB, Sheng G, Li X, et al. Crystalline 2D covalent organic framework membranes for high-flux organic solvent nanofiltration. *J Am Chem Soc*. 2018;140:14342-14349.

36. Xu WL, Fang C, Zhou F, et al. Self-assembly: a facile way of forming ultrathin, high-performance graphene oxide membranes for water purification. *Nano Lett.* 2017;17:2928-2933.
37. Li W, Wu W, Li Z. Controlling interlayer spacing of graphene oxide membranes by external pressure regulation. *ACS Nano.* 2018;12:9309-9317.
38. Nie L, Goh K, Wang Y, et al. Realizing small-flake graphene oxide membranes for ultrafast size-dependent organic solvent nanofiltration. *Sci Adv.* 2020;6:eaaz9184.
39. Wang Y, Wu N, Wang Y, et al. Graphite phase carbon nitride based membrane for selective permeation. *Nat Commun.* 2019;10:2500.
40. Feng Y, Weber M, Maletzko C, Chung T-S. Fabrication of organic solvent nanofiltration membranes via facile bioinspired one-step modification. *Chem Eng Sci.* 2019;198:74-84.
41. Wang Z, Tu Q, Zheng S, Urban JJ, Li S, Mi B. Understanding the aqueous stability and filtration capability of MoS₂ membranes. *Nano Lett.* 2017;17:7289-7298.
42. Shen J, Liu G, Huang K, Chu Z, Jin W, Xu N. Subnanometer two-dimensional graphene oxide channels for ultrafast gas sieving. *ACS Nano.* 2016;10:3398-3409.
43. Sapkota B, Liang W, VahidMohammadi A, Karnik R, Noy A, Wanunu M. High permeability sub-nanometre sieve composite MoS₂ membranes. *Nat Commun.* 2020;11:2747.
44. Hegab HM, Wimalasiri Y, Ginic-Markovic M, Zou L. Improving the fouling resistance of brackish water membranes via surface modification with graphene oxide functionalized chitosan. *Desalination.* 2015;365:99-107.
45. Koltonow AR, Huang J. Two-dimensional nanofluidics. *Science.* 2016;351:1395-1396.
46. Li D, Neumann AW. Equation of state for interfacial tensions of solid-liquid systems. *Adv Colloid Interface Sci.* 1992;39:299-345.
47. Xiao J, Wen H, Wang L, et al. Catalyst-free dehydrative SN1-type reaction of indolyl alcohols with diverse nucleophiles "on water". *Green Chem.* 2016;18:1032-1037.
48. Karan S, Jiang Z, Livingston AG. Sub-10 nm polyamide nanofilms with ultrafast solvent transport for molecular separation. *Science.* 2015;348:1347-1351.
49. Ahmad A, Li SH, Zhao ZP. Insight of organic molecule dissolution and diffusion in cross-linked polydimethylsiloxane using molecular simulation. *J Membr Sci.* 2021;620:118863.
50. Darvishmanesh S, Degreve J, Bruggen BVD. Mechanisms of solute rejection in solvent resistant nanofiltration: the effect of solvent on solute rejection. *Phys Chem Chem Phys.* 2010;12:13333-13342.
51. Huang K, Liu G, Lou Y, Dong Z, Shen J, Jin W. A graphene oxide membrane with highly selective molecular separation of aqueous organic solution. *Angew Chem Int Ed.* 2014;53:6929-6932.
52. Shen J, Liu G, Ji Y, et al. 2D MXene nanofilms with tunable gas transport channels. *Adv Funct Mater.* 2018;28:1801511.
53. Ma L, Gutierrez L, Vanoppen M, Lorenz DN, Aubry C, Verliefde A. Transport of uncharged organics in ion-exchange membranes: experimental validation of the solution-diffusion mode. *J Membr Sci.* 2018;564:773-781.
54. Holt JK. Fast mass transport through sub-2-nanometer carbon nanotubes. *Science.* 2006;312:1034-1037.
55. Nair RR, Wu HA, Jayaram PN, Grigorieva IV, Geim AK. Unimpeded permeation of water through helium-leak-tight graphene-based membranes. *Science.* 2012;335:442-444.
56. Gong X, Li J, Lu H, et al. A charge-driven molecular water pump. *Nat Nanotechnol.* 2007;2:709-712.
57. Hummer G, Rasaiah JC, Noworyta JP. Water conduction through the hydrophobic channel of a carbon nanotube. *Nature.* 2001;414:188-190.
58. Dou H, Jiang B, Xu M, et al. Boron nitride membranes with a distinct nanoconfinement effect for efficient ethylene/ethane separation. *Angew Chem Int Ed.* 2019;58:13969-13975.
59. Wang Y, Li L, Wei Y, et al. Water transport with ultralow friction through partially exfoliated g-C₃N₄ nanosheet membranes with self-supporting spacers. *Angew Chem Int Ed.* 2017;56:1-7.
60. Li J, Gong X, Lu H, Li D, Fang H, Zhou R. Electrostatic gating of a nanometer water channel. *Proc Natl Acad Sci U S A.* 2007;104:3687-3692.
61. Liu J, Wang N, Yu L, et al. Bioinspired graphene membrane with temperature tunable channels for water gating and molecular separation. *Nat Commun.* 2017;8:2011.
62. Zhang R, Li Y, Su Y, et al. Engineering amphiphilic nanofiltration membrane surfaces with a multi-defense mechanism for improved anti-fouling performances. *J Mater Chem A.* 2016;4:7892-7902.

SUPPORTING INFORMATION

Additional supporting information can be found online in the Supporting Information section at the end of this article.

How to cite this article: Chen C, Wu X, Zhang J, et al. Molecule transfer mechanism in two-dimensional heterostructured lamellar membranes: The effects of dissolution and diffusion. *AIChE J.* 2022;68(9):e17795. doi:10.1002/aic.17795